

ICFA BEAM DYNAMICS NEWSLETTER#85 —

CHALLENGES OF PRESENT AND FUTURE e^+e^- CIRCULAR COLLIDERS

Optics design and correction challenges for the high energy booster of FCC-ee

A. Chance,^a B. Dalena,^a T. Da Silva,^a A. Mashal,^b M. Migliorati,^{c,d} A. Ghribi,^{a,e,*} A. Rajabi^f and F. Zimmermann^g

^aCEA, IRFU

91191, Gif-sur-Yvette, France

^bSchool of Particles and Accelerators, Institute for Research in Fundamental Sciences (IPM),

P.O. Box 19395-5531, Tehran, Iran

^cUniversity of Rome La Sapienza

Piazzale Aldo Moro, 5, 00185 Roma RM, Italy

^dINFN Roma1,

Piazzale Aldo Moro, 5, 00185 Roma RM, Italy

^eCNRS, GANIL

Blvd Henri Becquerel, Caen, France

^fDeutsches Elektronen-Synchrotron DESY, Notkestr

85, 22607 Hamburg, Germany

^gCERN,

1211 Geneva 23, Switzerland

E-mail: adnan.ghribi@cea.fr

ABSTRACT: One of the major upcoming challenges in particle physics is achieving precise measurements of the Z, W, and H bosons, as well as the top quark. To meet these targets, the next e^+e^- collider complex, FCC-ee, will need to achieve unprecedented luminosities. The FCC-IS European Study is investigating the feasibility of these challenges, with a cornerstone of the study being the design and optimization of the high-energy booster (HEB). This paper provides an update on the status of the HEB of FCC-ee in light of recent developments in the injector and collider survey, as well as an overview of ongoing work on longitudinal stability and design robustness in relation to field, alignment, and diagnostics errors. Constraints and effects related to the design frequency of the accelerating cavities, as well as collective effects, are also highlighted. Lastly, the paper presents an investigation into an alternative arcs cell design.

KEYWORDS: Accelerator modelling and simulations (multi-particle dynamics, single-particle dynamics); Beam dynamics; Beam Optics

ARXIV EPRINT: [2304.00135](https://arxiv.org/abs/2304.00135)

*Corresponding author.

Contents

1	Introduction	1
2	Optics stability	2
3	Orbit correction	4
4	Collective effects and injection parameters	6
5	RF parameters and frequency choice	8
6	Momentum compaction tuning	9
7	Conclusion	10

1 Introduction

FCC-ee is a double-ring lepton collider and the first operational stage of the integrated long-term FCC project. It is expected to serve as an electron-positron Higgs and electroweak factory, achieving the highest luminosities within 15 years. There are four operational modes defined for FCC-ee, which are referred to as Z , W , H , and $t\bar{t}$. The beam properties, including energy, current, and emittance, vary for each mode. However, the short beam lifetime and the requirements for top-up injection are common features among them.

The High Energy Booster (HEB) is the final part of the injector complex, where particles with an energy of 20 GeV are injected into the HEB ring. The main criteria for the HEB lattice and its ramping cycle design are accelerating the particles up to the collision energy, adjusting beam properties for efficient top-up injection, and meeting filling time considerations.

Previous studies [1] have shown that a single design could not satisfy the mentioned requirements for all energies. Therefore, two distinguished lattices have been designed, one for Z and W modes and another for H and $t\bar{t}$ modes. Preliminary results confirmed the lattices' performance in the ideal case. However, in the realistic case, the HEB performance is affected by inevitable errors such as magnetic field imperfection and misalignment, instabilities raised from collective effects, and the behavior of particles during the ramping process. Hence, it is necessary to ensure the possibility of correcting destructive effects before finalizing the design.

The effects of magnetic multipole errors on lattice momentum acceptance and a first analytical estimation of emittance growth in the presence of intra-beam scattering have been previously reported [2]. This paper is a status report on the aforementioned developments for the HEB design. The second section reports on the study of longitudinal phase space stability, while the third section details closed orbit correction strategies in the presence of misalignment errors. The fourth section shows the beginning of a joint effort for precise collective effects studies. Section six provides an update on the

change in RF cavities frequencies with respect to the Conceptual Design Report and the corresponding RF budget. Finally, an alternative optics design under study is presented in the last section.

2 Optics stability

One of the ongoing tasks is to achieve sufficiently large Dynamic Aperture (DA) and Momentum Aperture (MA) for a 90° phase advance lattice, designed for modes H , tt and $t\bar{t}$. By using a non-interleave sextupoles arrangement with 32 pairs of focusing sextupoles and 33 pairs of defocusing sextupoles in each arc, a considerably large on momentum dynamic aperture (in absence of the radiation and RF cavities) is obtained, when longitudinal motion is considered (with RF cavities) the on-momentum dynamic aperture is greatly reduced, as shown in figure 1. Increasing the number of sextupole families to four and optimizing resonance driving terms enhances the DA, especially for off-momentum particles. The size of both the DA and MA is reduced when a 6D tracking procedure includes radiation effects and energy compensation at RF cavities.

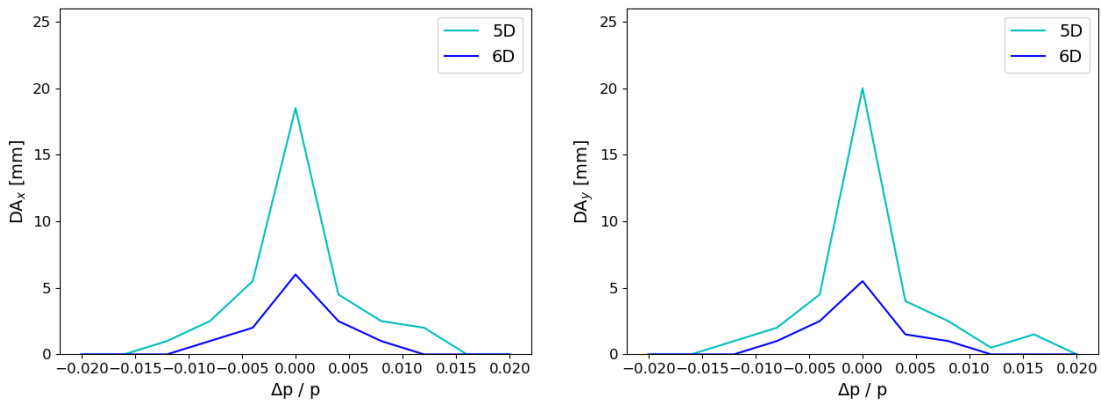


Figure 1. Horizontal (left) and vertical (right) Dynamic Aperture as a function of momentum deviation for non-interleave sextupoles arrangement with 32 pairs of focusing sextupoles and 33 pairs of defocusing sextupoles in each arc.

As a first step in resolving this issue, we investigate particles' stability in the longitudinal phase space. A kilometer-scale bending radius of the dipole magnets, as well as the low value of dispersion function along them, makes the lattice's momentum compaction factor to become very small. In this case, even a slight perturbation in momentum compaction could lead to instability in the longitudinal phase space. A variation in path length with momentum at higher order could be used to compute perturbation terms [3] as equation (2.1) shows:

$$\frac{\Delta L}{L_0} = \alpha_c \delta + \alpha_1 \delta^2 + \xi + \mathcal{O}(3) \quad (2.1)$$

where L_0 is the nominal path length, α_c the momentum compaction factor, $\eta_c = 1/\gamma^2 - \alpha_c$ the slipping factor, γ the Lorentz boost, α_1 the second order momentum compaction and ξ the momentum independent term (see [3] for more details). The extended form of the momentum compaction in the Hamiltonian reveals the existence of the secondary RF bucket in the longitudinal phase space.

For certain condition which depends on perturbation terms α_1 and ξ , these buckets could get close and interfere with each other. The buckets' interference disturbs the longitudinal phase stability condition and reduces the momentum acceptance of the lattice. Moreover, the width of the RF buckets determines by the desired momentum acceptance and its required RF voltage. Hence, the stability criterion for the perturbation term α_1 as a function of desired momentum acceptance could be defined [3] as in equation (2.2):

$$\alpha_1 \leq \frac{|\eta_c|(1-\Gamma)^{3/4}}{\sqrt{3}(\Delta p/p_0)_{\text{desired}}} \quad \text{Where } \Gamma = \frac{4\xi\alpha_1}{\eta_c^2} \quad (2.2)$$

Tracking the on-axis particle within the momentum acceptance range of the ideal lattice gives us $\alpha_c = 7.33 \times 10^{-6}$, $\alpha_1 = 3.52 \times 10^{-6}$, and $\xi = 3.07 \times 10^{-11}$; so, the right hand side of equation (2.2) for desired $\pm 5\%$ momentum acceptance is equal to 8.46×10^{-5} and the lattice meets this stability condition. The location of the primary and secondary RF buckets in the longitudinal phase space is shown in figure 2. It should be noted that the secondary RF buckets are situated at a considerable distance from the main buckets, and their influence on the particle dynamics can be disregarded.

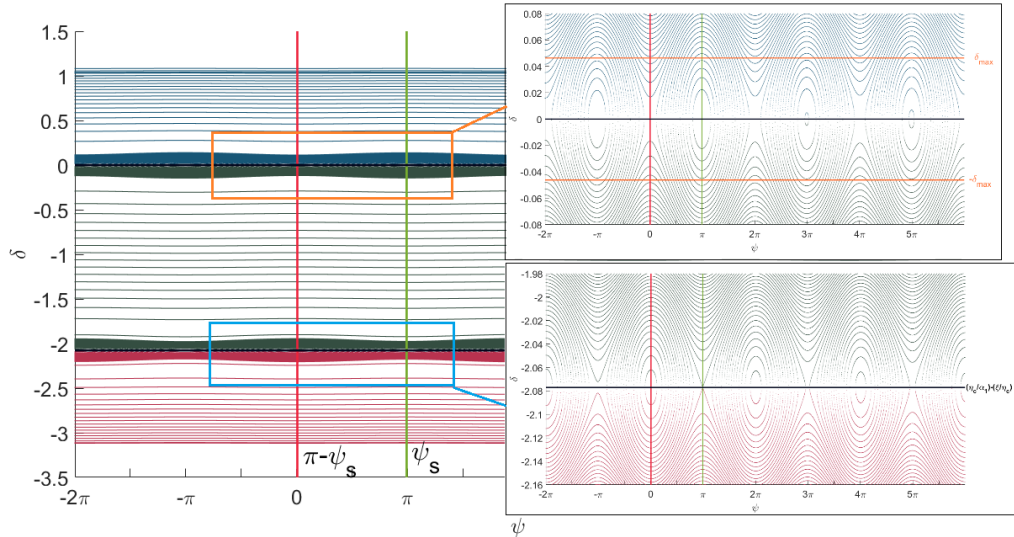


Figure 2. The location of primary and secondary RF buckets in longitudinal phase space.

The initial amplitude of the particle could alter the first and second-order momentum compaction factors as well as the momentum-independent path length variation. Although, for an on-axis bunch the amplitude of the betatron oscillation varies within the range of transverse beam size. In this case, α_c and ξ will remain constant and only the variation of α_1 with respect to the amplitude could affect synchrotron oscillation stability. Accordingly, a stability criterion for variation of α_1 has been defined in [3] as $\Delta\alpha_1 < \frac{\eta_c^2}{4\xi} = 0.226$. Figure 3 shows the variation of α_1 in the range of ± 1 [mm]. This area would be several times greater than the beam size in all possible injection scenarios. The result shows the stability of synchrotron oscillation within this area.

In order to investigate the effect of higher-order momentum compaction on the DA we have to consider greater initial amplitudes so the variation of α_c and ξ has to be taken into account. The

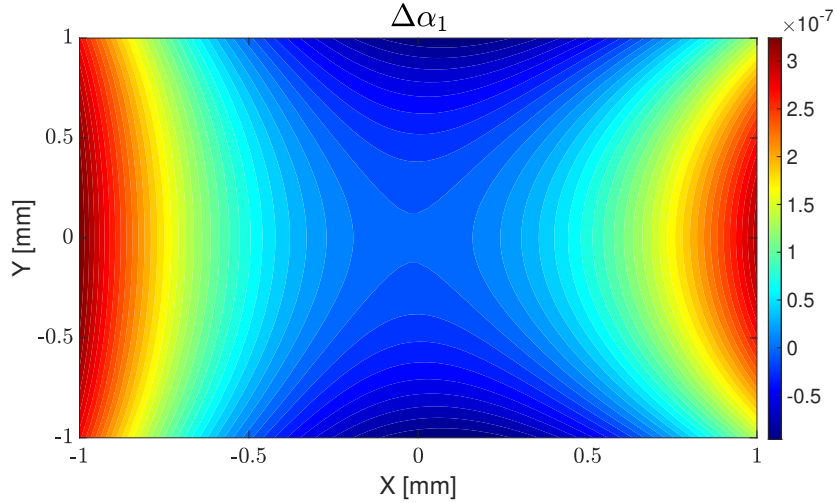


Figure 3. The variation of α_1 for the different amplitudes.

stability criteria for each point would be defined as $\frac{4\xi\alpha_1}{|\eta_c|^2} < 1$. The area of the region of stable synchrotron oscillation along with the on-momentum DA is shown in figure 4.

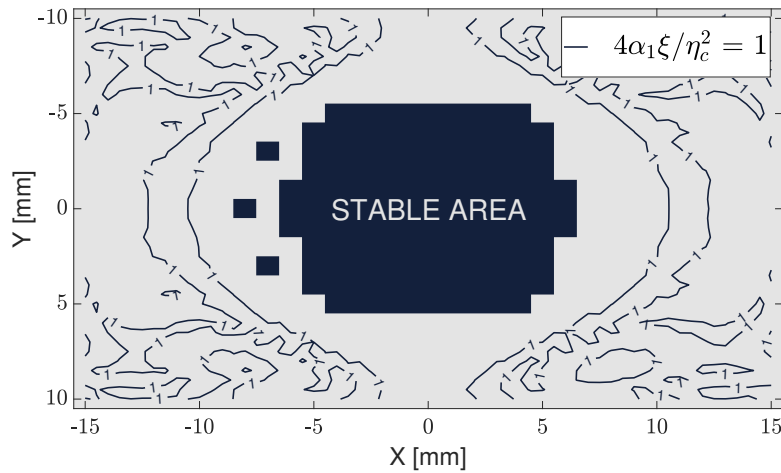


Figure 4. The stable area is the DA of on-momentum particles for 6D tracking and the lines show the border of stable synchrotron motion.

The DA obtained from 5D tracking exceeds the defined border of synchrotron oscillation stability. In contrast, the DA in the 6D tracking case remains within the border. Hence, it could be concluded that the instability raised by the higher-order momentum compaction factor is one of the main reasons for diminishing the DA in the presence of RF cavities.

3 Orbit correction

The objective of the orbit correction study is twofold: firstly, to establish the permissible tolerances for the misalignment of the booster's components, and secondly, to assess the necessary strength of

the correctors to rectify the closed orbit perturbation resulting from machine errors. Various types of errors have been taken into account, including random dipole field and roll errors, quadrupole alignment errors, BPM alignment and reading errors, and sextupole alignment errors.

The correction strategy described in ref. [4] was employed to evaluate the tolerances for misalignment and field errors on the elements. To do so, we conducted several tests by gradually introducing different error types, each on 100 seeds. The initial test configuration consisted of the combination of quadrupole offsets (MQ), dipole relative field error (MB), and main dipole roll error. Statistical analysis of this initial configuration revealed that the proposed correction strategy converges for all seeds until an MQ offset of $150\ \mu\text{m}$ is reached. Notably, all errors applied to the elements are randomly Gaussian distributed within ± 3 RMS (Root Mean Square).

Figure 5 shows the orbit and correctors strengths values and distributions with their respective analytical RMS values for the 99 successful seeds at the end of the correction procedure. The dashed red lines on the distributions represents the RMS calculated analytically.

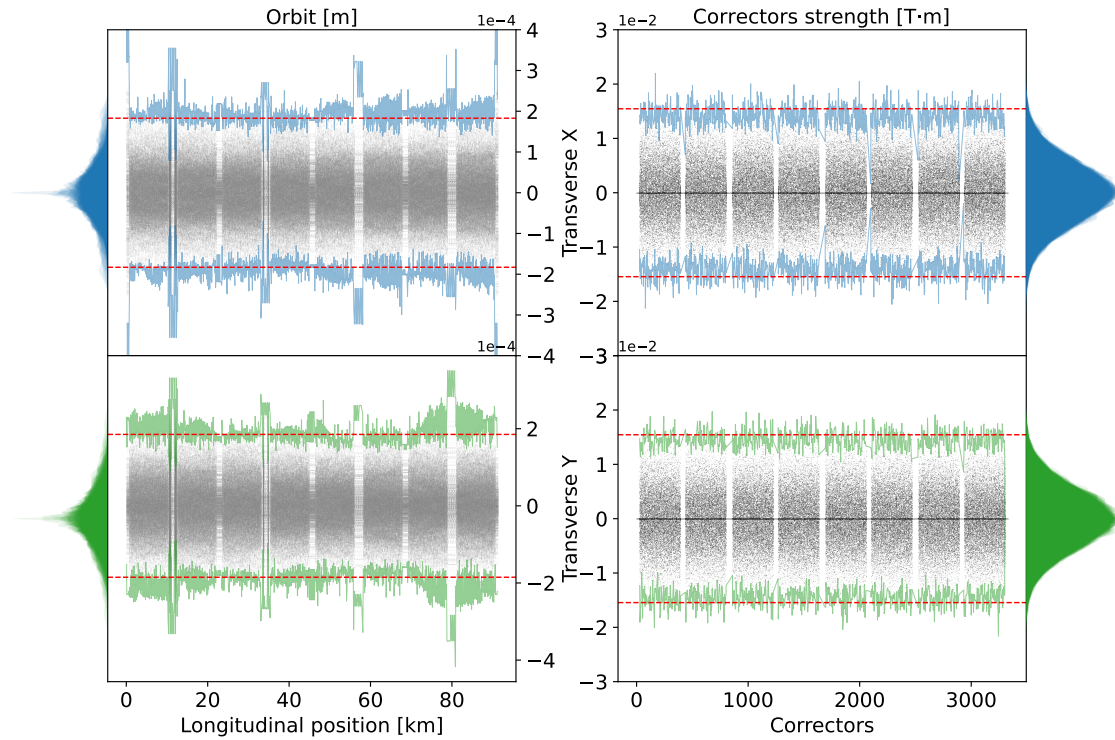


Figure 5. Superposition of the orbits and the correctors strengths of 99 seeds (dots) and the global envelope for all considered machine configurations (solid line) in the X and Y transverse planes. Density distributions (one for each seed) are also superposed. The red dashed line is 3 times the mean of the analytical RMS values.

In both the orbit and the corrector strength analyses, we observe that our analytical predictions align well with the simulation data. Specifically, the estimation accurately captures all the data for the vertical plane, while the horizontal plane has a few outliers that exceed the analytical limit. These behaviors can be explained by the combined effect of different errors and the β -function, which renders the procedure less effective. Nonetheless, the orbit distribution corresponds to our expectations, with the amplitude in both planes being in the order of magnitude of the MQ offsets (the

dominant errors). Moreover, the pattern of the succession of the arcs and insertions is apparent, as we only applied the errors on the arcs, and the residual orbit after correction in the insertions should be almost zero. The RMS values for each successful seed are distributed around the dashed red line representing one analytical RMS estimate. The blue dots correspond to the RMS after turning on the sextupoles and correcting the orbit once, always using a Singular Value Decomposition (SVD) algorithm. Few outlier seeds exist that do not improve with the iteration of the corrector procedure.

Regarding the correctors' strength distribution (see figure 5), we observe that the strengths are contained in the 3 times mean analytical RMS limit. Therefore, the first specifications for the main magnets' misalignment of the High Energy Booster arcs cells are set to 150 μm , with a maximum corrector strength of about 20 mT m, as far as orbit correction is concerned. These values will be confirmed or potentially reduced following the full emittance tuning performance study.

4 Collective effects and injection parameters

The high energy booster's smaller pipe radius of 25 mm, compared to the collider's 35 mm, and almost 100 km circumference, along with the required injection energy and bunch population for the desired emittance at different operating modes (shown in table 1), make collective effects important. Two of these effects being investigated are the resistive wall and intrabeam scattering (IBS).

As for the resistive wall, because of the reduced pipe diameter, the impedance and the wakefield contributions are expected to be higher than the main rings [5, 6] in both longitudinal and transverse plane.¹

Another important point related to the resistive wall is the possible presence of eddy currents that could be generated by the ramp of the magnetic field during acceleration. In order to avoid them, an initial proposal of a stainless steel vacuum chamber was discussed. This material would have increased the resistive wall contribution by a too large amount. However, due to the low magnetic field in the booster,² the Eddy currents are not expected to be a problem, giving, as consequence, that it is possible to have a stainless steel vacuum chamber with a copper coating of 1 mm, so that, from about 2 kHz on, the skin depth is such that the beam sees only the copper. However, one simple way to fabricate such a vacuum chamber would give, as a final result, a copper pipe with a stainless steel strip about 1 mm wide³ seen by the beam. This strip would produce an azimuthal asymmetry in the impedance and this contribution, also taking into account the detuning (quadrupolar) terms, has to be studied in detail. In this section, we present only preliminary results for a circular beam pipe made of copper. The longitudinal and transverse wake potentials of a 0.2 mm Gaussian bunch used as a pseudo-Green function for copper and stainless steel are shown in figure 6.

With such contributions, the effects on beam dynamics have been studied with the PyHEADTAIL tracking code [7]. As initial conditions for the bunch distribution we have supposed a transverse emittance of 300 pm in the horizontal plane and 1.4 pm in the vertical plane, with an equilibrium relative energy spread of 3×10^{-4} and a zero current bunch length of about 2.2 mm.

¹These two effects scale as r^{-1} in the longitudinal plane and as r^{-3} in the transverse one.

²According to the CDR [1] from 0.007 T at 20 GeV to a maximum peak of 0.046 T at 182.5 GeV, with a rate of field change below 0.03 T/s.

³Private communication.

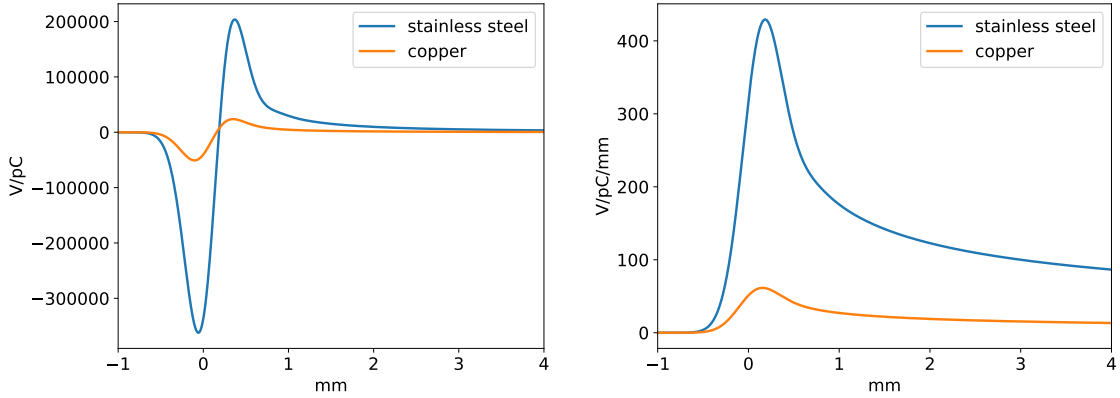


Figure 6. Illustration of longitudinal (left) and transverse dipolar (right) wake potential of a 0.2 mm Gaussian bunch for a copper and stainless steel vacuum chamber.

The effect of the longitudinal wakefield is shown in figure 7 (right). We can see that, at the nominal bunch population of 2.4×10^{10} we have an effect of the potential well distortion, but also a slight microwave instability which increases the energy spread by a few percents with respect to its nominal value.

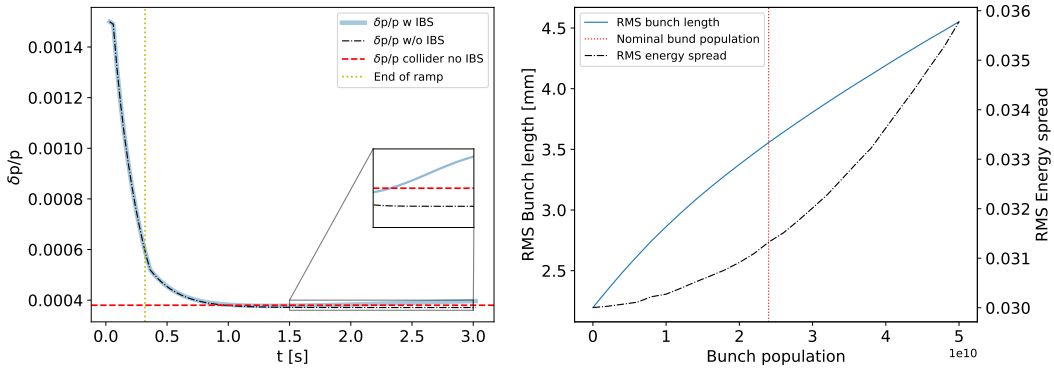


Figure 7. Left: effect of the IBS on the evolution of the energy spread during a linear ramp for an injected beam energy spread and bunch length respectively set to 0.15% and 1 mm. Right: rMS bunch length and energy spread versus bunch population.

In the transverse plane, the wakefield can produce Transverse Mode Coupling Instability (TMCI), which can be more dangerous than microwave instability because it can cause beam loss. The instability occurs when two coherent oscillations modes couple together. As shown in figure 8 [8], the threshold is higher than the nominal current. However, we need to keep some safety margin because all possible effects like collimator, RF cavity impedances, or bellows are not included yet.

It is important to note that the presented results provide only a rough evaluation of the collective effects on the beam dynamics of the booster. Self-consistent simulations that take into account the intrabeam scattering and wakefields, both influencing the bunch length, must be considered. Additionally, the possible difference in the resistive wall impedance due to the presence of the strip,

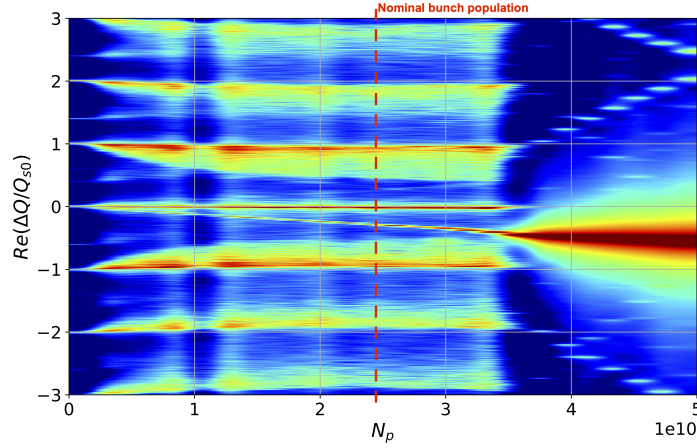


Figure 8. Real part of the tune shift of the first azimuthal transverse coherent oscillation modes normalised by the synchrotron tune Q_{s0} as a function of bunch population. The nominal bunch population is shown in dashed red line.

which produces also an asymmetry with contributions to the detuning (quadrupolar) impedance, must be carefully evaluated. Finally, the machine impedance model has to be built. For the IBS, an updated analytical study made with MadX with respect to the one published in [2] is represented in figure 7 (left). It shows an important contribution of the IBS after energy ramp to the energy spread making it higher than the collider threshold. This result is however to be confirmed with tracking simulation taking into account simultaneously the wakefield and the IBS.

5 RF parameters and frequency choice

As the HEB is central in the accelerator complex design, it provides inputs to the different working group studies. One of these inputs is the radiofrequency (RF) total voltage budget, which depends, among other things, on the bunch length needed at extraction for different energy modes and the RF frequency of the accelerating cavities. Recently, the base design of the RF frequency has changed from 400 MHz to 800 MHz, requiring a revision of the total voltage budget. Assuming no energy gain ($E_{\text{gain}} = 0$), one can calculate the resulting RF voltage using the Equation (5.1):

$$V_{\text{RF}} = \sqrt{\left(\frac{C^2 \sigma_e^2 E_t \eta}{2\pi \nu_{\text{RF}} \sigma_z^2 \beta^3}\right)^2 + (E_{\text{gain}} + U_0)^2} \quad (5.1)$$

In this equation, C represents the booster circumference, σ_z is the bunch length, E_t is the total energy, $\eta \approx -\alpha_c$ is the slippage factor, β is the normalized velocity, ν_{RF} is the RF cavities frequency, U_0 is the synchrotron energy loss per turn, and σ_e is the energy spread.

At injection energy, the momentum acceptance is taken as a criterion for the calculation of the cavities RF voltage budget by solving Equation (5.2):

$$\delta_p = \frac{2Q_s(V_{\text{RF}})c}{C\nu_{\text{RF}}\alpha_c} \sqrt{\tan \phi_s(V_{\text{RF}}) * (1 + \phi_s(V_{\text{RF}}) - \pi/2)} \quad (5.2)$$

with $Q_s(V_{\text{RF}})$ the synchronous tune and $\phi_s(V_{\text{RF}})$ the synchronous phase.

Table 1. Total RF voltage budget for the different energy modes of the FCC-ee HEB for two RF cavities frequencies.

Modes	Injection 60° ^a /90° ^b	Z	W	H	$t\bar{t}$	[Units]
Energy	20	45.6	80	120	182.5	[GeV]
σ_z ^c	4	4.38	3.55	3.34	1.94	[mm]
δ_p ^d	3	4.38	3.55	3.34	1.94	[mm]
α_c ^e	14.9 / 7.34		14.9		7.34	[10 ⁻⁶]
$V_{RF,400}$ ^f	53.6 / 27.6	124.6	1023.2	2185.6	14205.4	[MV]
$V_{RF,800}$ ^g	104.8 / 52.8	83.9	623.6	2038.3	11554.9	[MV]

^a60° phase advance lattice of the Z and W modes.

^b90° phase advance lattice of the H and $t\bar{t}$ modes.

^cBunch length.

^dMomentum acceptance.

^eMomentum compaction factor.

^fRF voltage for $\nu_{RF} = 400$ MHz.

^gRF voltage for $\nu_{RF} = 800$ MHz.

As can be seen in table 1, the frequency change from 400 MHz to 800 MHz allows to reduce the total cavities RF budget required at extraction. However, taking the momentum acceptance as a requirement at injection almost doubles it when the RF frequency is doubled.

6 Momentum compaction tuning

In the baseline, the arcs are made of FODO cells with a phase advance of 60°/90° respectively for the modes Z/W and $H/t\bar{t}$. The main reason is a larger momentum compaction at injection at the Z/W modes to manage stronger collective effects due to a larger current. However, to enlarge the dynamic aperture, the sextupole scheme is based on a non-interleaved scheme with a phase advance of 180° between two sextupoles of a pair. Maintaining the possibility to have 60°/90° implies to have a different cabling for the different operation modes. Moreover, the number of sextupoles is roughly doubled.

We propose to tune the momentum compaction by keeping the same non-interleaved scheme for all operation modes. The principle is to create a dispersion and betatron wave at one quadrupole near a sextupole. We assume for instance that the integrated quadrupole strength is modified by Δk ; the quadrupole near the other paired sextupole is modified by $-\Delta k$ (see figure 9). The phase advance between the center of the 2 quadrupoles is 180° in both planes. By this way, the betatron wave is cancelled in the second quadrupole contrary to the dispersion wave (because the frequency of the betatron wave is twice the one of the dispersion wave). The other advantage is also not to change the tune of the cell. If we do the thin lens approximation then to get a relative change of x on the momentum compaction, we should have $\Delta k \approx \frac{\sqrt{x}}{2\sqrt{3}}$

An example of the reference 90° FODO cell and the alternative optics with a doubled momentum compaction is shown in figure 10. The consequence is to get a I_5 ratio of 6.25, to be compared with a ratio of 3 if we use 60° FODO cells.

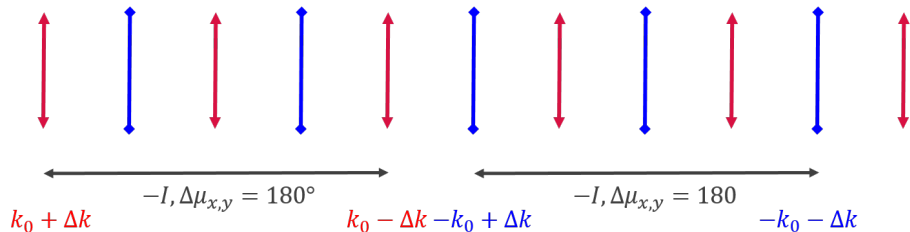


Figure 9. Scheme to tune the momentum compaction. The focusing/defocusing quadrupoles are respectively in red/blue.

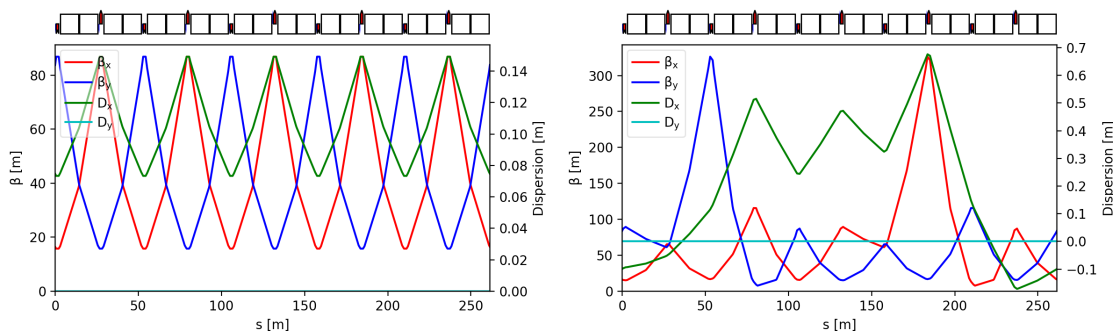


Figure 10. Optics in the cell with no dispersion bump (left) and with a dispersion bump to double the momentum compaction (right).

The advantages of this scheme are to simplify the cabling and distribution of the sextupoles in the arcs; to enable to tune the momentum compaction during the ramp and thus to get a smaller equilibrium emittance for the Z/W modes; to be compatible with any arc pattern if the phase advance between the sextupoles is still 180° . The drawbacks are an additional power supply for the quadrupoles (but that should be less expensive than increasing the number of sextupoles if we have to keep non-interleaved scheme for $60^\circ/90^\circ$ cells), a larger equilibrium emittance in comparison with a FODO cell giving the same momentum compaction, a possible reduction of the dynamic aperture and momentum acceptance.

7 Conclusion

This paper reports on the status of several ongoing parallel developments for the FCC-ee High Energy Booster. One of the ongoing studies focuses on particle stability in longitudinal phase space, particularly with regard to the control of synchro-betatron excitations and increase the off-momentum DA. To this purpose, a different optics design and best settings of main sextupoles need to be further investigated. Other investigations are aimed at evaluating the performance of the HEB optics design, in particular with respect to stability against lattice elements imperfections, main sextupoles settings, and the interplay of collective effects with a realistic lattice model. By integrating Wakefield and IBS, together with synchrotron radiation, we aim to gain important insights into the injection parameter constraints. These simulations will also allow us to compare the effects of different energy ramping strategies.

All these studies will provide input for alternative optics design and RF parameter choices for the different operating modes, while maintaining compatibility with both pre-injectors and collider requirements. However, it is important to note that these studies are highly dependent on various inputs such as accelerating cavities RF frequency, bunch population, vacuum pipe geometry, material and coating, and collider length, among other parameters. Therefore, they must be conducted in parallel and in dynamic interaction with other ongoing studies such as pre-injectors, collider optics, radio-frequency, or arcs optics patterns to ensure that all the necessary inputs are taken into consideration, and that the most optimal solutions are achieved.

Acknowledgments

This work was supported by the European Union’s Horizon 2020 Research and Innovation programme under grant no. 951754 (FCCIS).

References

- [1] FCC collaboration, *FCC-ee: The Lepton Collider: Future Circular Collider Conceptual Design Report Volume 2*, *Eur. Phys. J. ST* **228** (2019) 261.
- [2] B. Dalena, A. Chance, F. Antoniou, O. Etisken, A. Mashal, T. Raubenheimer et al., *Status of the High Energy Booster of the lepton option of the future circular collider*, *PoS ICHEP2022* (2022) 042.
- [3] H. Wiedemann, *Particle Accelerator Physics*, Graduate Texts in Physics, Springer, Berlin, Germany (2015), [10.1007/978-3-319-18317-6](https://doi.org/10.1007/978-3-319-18317-6).
- [4] B. Dalena, T. Da Silva, A. Chance and A. Ghribi, *Definition of tolerances and corrector strengths for the orbit control of the High-Energy Booster ring of the future electro-positron collider*, in proceedings of the 14th International Particle Accelerator Conference, Venice, Italy, 7–12 May 2023, pp. 646–649 [arXiv:2303.17996](https://arxiv.org/abs/2303.17996).
- [5] M. Migliorati, E. Belli and M. Zobov, *Impact of the resistive wall impedance on beam dynamics in the Future Circular e^+e^- Collider*, *Phys. Rev. Accel. Beams* **21** (2018) 041001.
- [6] M. Migliorati, E. Carideo, D. De Arcangelis, Y. Zhang and M. Zobov, *An interplay between beam–beam and beam coupling impedance effects in the Future Circular e^+e^- Collider*, *Eur. Phys. J. Plus* **136** (2021) 1190.
- [7] K. Li, H. Bartosik, S. Hegglin, G. Iadarola, A. Oeftiger, A. Passarelli et al., *Code development for collective effects*, in proceedings of the 57th ICFA Advanced Beam Dynamics Workshop on High-Intensity and High-Brightness Hadron Beams, Malmö, Sweden, 3–8 July 2016, 362–367.
- [8] E. Métral and M. Migliorati, *Longitudinal and transverse mode coupling instability: Vlasov solvers and tracking codes*, *Phys. Rev. Accel. Beams* **23** (2020) 071001.